



1 **Formation of Highly Absorptive Secondary Brown Carbon Through Nighttime**
2 **Multiphase Chemistry of Biomass Burning Emissions**

3 **Ye Kuang^{1,*}, Biao Luo¹, Shan Huang^{1*}, Junwen Liu¹, Weiwei Hu², Yuwen Peng¹, Duohong Chen³,**
4 **Dingli Yue³, Wanyun Xu⁴, Bin Yuan¹, Min Shao¹**

5 ¹ Institute for Environmental and Climate Research, College of Environment and Climate, Jinan
6 University, Guangzhou, China.

7 ² State Key Laboratory of Organic Geochemistry and Guangdong Key Laboratory of Environmental
8 Protection and Resources Utilization, Guangzhou Institute of Geochemistry, Chinese Academy of
9 Sciences, Guangzhou 510640, China

10 ³ Guangdong Ecological and Environmental Monitoring Center, State Environmental Protection Key
11 Laboratory of Regional Air Quality Monitoring, Guangzhou 510308, China

12 ⁴ State Key Laboratory of Severe Weather, Key Laboratory for Atmospheric Chemistry, Institute of
13 Atmospheric Composition, Chinese Academy of Meteorological Sciences, Beijing, China

14

15 Corresponding author: Ye Kuang (kuangye@jnu.edu.cn) and Shan Huang

16 (shanhuang_eci@jnu.edu.cn)

17

18

19

20

21

22

23

24



25 **Abstract**

26 Biomass burning is a major global source of both primary brown carbon (BrC) and reactive trace
27 gases in the atmosphere, thus exerts significant impacts on global climate and regional atmospheric
28 chemistry. However, a substantial gap remains in our understanding of the nighttime evolution of
29 biomass burning emissions. Here we present prominent nighttime formation of secondary organic
30 aerosol (Night-OA) with strong absorptivity but markedly different spectral dependence from that of
31 primary biomass burning organic aerosols, which was observed during autumn of the Pearl River Delta
32 region of China when biomass burning plumes prevailed. Our results demonstrate that the formation
33 of Night-OA appeared high dependence on both magnitudes of afternoon biomass burning emissions
34 and available oxidants of NO₂ and O₃. Active nighttime NO₃ radical chemistry was characterized by
35 quick O₃ depletion and almost zero concentration of NO, and the rapid decrease of NO₂ coincident
36 with the quick nitrate formation suggests that the rapid NO₂ consumption supplied the NO₃ and N₂O₅
37 reaction chains. However, the quickest Night-OA formation occurred when nitrate formation ceased
38 and relative humidity reached maximum, and mainly added mass to aerosol water abundant diameter
39 ranges. This co-variation demonstrates that gas-phase and aqueous-phase chemistry of biomass
40 burning precursors likely coordinated to promote the quick nighttime formation of Night-OA. Findings
41 of this study highlight the nighttime darkening of biomass burning plumes through multiphase
42 reactions and the proposed secondary BrC formation mechanisms may have broad implications in
43 climate and air quality effects of biomass burning, such as the interaction between biomass burning
44 plumes with water abundant pyroconvection cloud.

45

46

47

48

49

50

51

52

53



54 **1 Introduction**

55 Light absorbing organic aerosols termed as brown carbon (BrC) (Andreae and Gelencsér, 2006),
56 absorbs solar radiation and warms the atmosphere, acts as potential photosensitizers and alters
57 atmospheric oxidation capacity (Liu et al., 2020), thus impacting profoundly on atmospheric chemistry,
58 air quality and climate (Jo et al., 2016). Biomass burning activities happen frequently across the globe
59 due to natural and anthropogenic activities, injecting large amounts of fine organic aerosols (known as
60 biomass burning organic aerosol, BBOA) and trace gases into the global atmosphere, thereby acting
61 as a major global source of atmospheric primary organic aerosols and non-methane volatile organic
62 compounds (Andreae and Merlet, 2001; Akagi et al., 2011; Andreae, 2019; van der Werf et al., 2017),
63 thus exerting significant impacts on global climate (Liu et al., 2021; Yu et al., 2019; Yu et al., 2021).
64 The freshly emitted BBOA is highly absorptive near ultraviolet wavelengths and considered as a major
65 contributor to atmospheric BrC (Wang et al., 2016). A number of laboratory studies revealed that
66 secondary organic aerosol (SOA) formed from the oxidation of biomass burning precursors (BBSOA)
67 is also absorptive (Saleh et al., 2013), however, the importance of secondary BrC formed from biomass
68 burning precursors remains uncertain.

69 Both daytime and nighttime chemistry play significant roles in aging biomass burning plumes
70 and associated secondary SOA and BrC formation. Daytime aging of biomass burning emissions and
71 its impacts on SOA formations have previously been extensively investigated (Hodshire et al., 2019),
72 which found that the formed SOA contributed substantially to BrC (Kumar et al., 2018; Saleh, 2020)
73 and confirmed by field measurements. For example, Palm et al. (2020) observed that daytime oxidation
74 of emitted phenolic compounds contributed a majority to BBSOA formation, with products being
75 highly absorptive. Compared with daytime aging experiments of biomass burning emissions,
76 laboratory studies representative of night chemistry are scarce. At night, the consumptions of O₃ and
77 OH is much faster than their formation rates due to the absence of photochemical reactions, thus
78 atmospheric concentration of these two oxidants reduce rapidly after sunset. The depletion of O₃
79 through NO₂ oxidation generates NO₃ radical that act as a major oxidant during nighttime periods and
80 drives the tropospheric nighttime chemistry. Decker et al. (2019) investigated the nighttime chemical
81 transformation in biomass burning plumes using a box model, which was initialized by aircraft
82 observations, with results demonstrating NO₃ radical loss mostly due to reactions with biomass



83 burning volatile organic compounds (VOCs). In recent years, a number of laboratory studies using
84 NO_3 as oxidant were carried out to explore influences of nighttime aging on biomass burning emissions
85 related SOA formations and associated BrC evolutions (Cheng et al., 2020; Li et al., 2020a; Jiang et al.,
86 2019; Tiitta et al., 2016; Hartikainen et al., 2018). Their results demonstrated that both nighttime aging
87 of BBOA aerosols and biomass burning VOC precursors such as pyrrole can potentially act as
88 important sources of SOA and BrC. However, contributions derived from laboratory studies cannot
89 be directly linked with SOA and BrC contribution magnitudes within ambient nighttime atmosphere.
90 Kodros et al. (2020) further highlighted the importance of nighttime processing of biomass burning
91 emissions as an important global source of SOA based on combined results from laboratory and field
92 observations. Nevertheless, field measurements that observed nighttime evolutions of biomass burning
93 plumes and directly confirmed significant contributions of SOA and BrC from nighttime aging of
94 biomass burning emissions are highly in lack. Only one field measurement study has observed
95 substantial increase of BrC light absorption during a night-long biomass burning event and identified
96 nitroaromatics in abundance within aged BBOA aerosols, contributing greatly to light absorption (Lin
97 et al., 2017; Bluvshstein et al., 2017), based on which it was hypothesized that nighttime chemistry
98 involving NO_3 radical oxidation of primary BBOA might play significant roles in BrC transformation.
99 Nighttime conditions are typically characterized by high atmospheric relative humidity (RH) caused
100 by temperature decreases, therefore likely result in abundant aerosol water, which might favor aqueous
101 SOA and BrC formation (Wang et al., 2019b). However, most of previous laboratory studies have not
102 investigated the role of RH or aqueous phase chemistry in nighttime aging of biomass burning plumes.
103 Kodros et al. (2022) found that nighttime oxidation of biomass burning emissions were sensitive to
104 RH, however, could not conclude what roles RH was. Their results demonstrated that homogenous
105 gas-phase oxidation and subsequent condensation of lower-volatility vapors was probably the
106 dominant process, however, they could not rule out the possible role of heterogeneous oxidation
107 processes. Therefore, how nighttime NO_3 radical chemistry coordinates with aerosol aqueous or
108 heterogenous reactions under high nighttime RH conditions to affect SOA and BrC formations remains
109 unexplored, which is a substantial knowledge gap in the research field of nighttime chemical
110 transformation of biomass burning emissions and its role in SOA and secondary BrC formations.

111 In this study, we report substantial amounts of highly absorptive SOA likely formed during
112 nighttime mainly from biomass burning emissions. The potential formation mechanisms of nighttime



113 SOA formation are investigated based on real-time measurements of parameters such as gaseous
114 pollutants, aerosol physical and chemical properties and meteorological factors. Our results revealed
115 that coordinated nighttime multiphase chemistry of biomass burning emissions likely formed highly
116 absorptive SOA, which improved our current understanding on nighttime aging of biomass burning
117 emissions and might also have significant implications for cloud processing of biomass burning.
118 Additionally, this study is a companion paper to Luo et al. (2022), where we proposed an improved
119 absorption Ångström exponent (AAE) ratio method for deriving multiwavelength BrC absorptions
120 from multiwavelength aerosol absorption measurements using an aethalometer, and investigated
121 comprehensively size distribution, absorption and scattering as well refractive index of primary BBOA.

122 **2 Materials and Methods**

123 **2.1 Field measurements**

124 A field campaign was conducted from 30 September to 17 November 2019 at a regional
125 background site of the Peral River Delta region. This site locates at the country side of Heshan county,
126 about 55 km away from the megacity Guangzhou and at the top of hill with surroundings are small
127 villages and residential towns. Routine observations of air pollutants such as carbon monoxide, ozone
128 nitrogen dioxides and PM_{2.5} (particulate matter with aerodynamic diameter less than 2.5 μm), and
129 meteorological parameters such as air relative humidity (RH), temperature, wind speeds and directions
130 were managed by the provincial environmental monitoring authority and this site is authorized as a
131 regional background supersite. During the observation period, intensive aerosol measurements
132 including aerosol optical properties, aerosol size distributions as well as aerosol chemical compositions
133 were also performed to investigate relationships between aerosol physical properties and aerosol
134 chemical compositions. The aerosol scattering properties and aerosol hygroscopicity were measured
135 using a humidified nephelometer (Aurora 3000) system (Kuang et al., 2021). Aerosol absorptions of
136 multiple wavelengths were measured using an aethalometer (Magee AE33, (Drinovec et al., 2015)).
137 Aerosol size distributions were measured jointly by using a scanning mobility particle sizer (SMPS,
138 TSI 3080) and an aerodynamic particle sizer (APS; TSI Inc., Model 3321). More details on the site
139 and set-up of instruments please refer to Kuang et al. (2021) and Luo et al. (2022).

140 The submicron aerosol chemical compositions were measured using a soot particle high-
141 resolution time of flight aerosol mass spectrometer (SP-AMS, Aerodyne Research, Inc., Billerica, MA,



142 USA). The set-up and validation of SP-AMS measurements were performed and discussed in Kuang,
143 et al. (Kuang et al., 2021), thus not detailed here. Source identification of organic aerosols was
144 performed using the commonly used positive matrix factorization (PMF), two primary OA factors and
145 four secondary OA factors are identified, and the determination of PMF factors are thoroughly
146 discussed in Luo et al. (2022). The two primary OA factors include biomass burning organic aerosols
147 (BBOA) and a hydrocarbon-like organic aerosols (HOA). The biomass burning emissions represent
148 the most important primary sources during the observations as discussed in Luo et al. (2022), and its
149 most prominent activities were usually observed near sunset (Fig.1a). The four SOA factors including
150 more oxygenated organic aerosols (MOOA, O/C=1), less oxygenated organic aerosols (LOOA,
151 O/C=0.72), nighttime-formed organic aerosols (Night-OA, O/C=0.32) and aged BBOA (aBBOA,
152 O/C=0.39). The Night-OA factor was characterized by its obvious correlation with nitrate and they
153 both exhibited obvious increase after sunset (Fig.1a). The name of aBBOA was originally because of
154 its correlation with $C_6H_2NO_4^+$ which is a typical fragment of the aged BBOA component nitrocatechol
155 (Bertrand et al., 2018). The mass spectral profiles and time series of these organic aerosol factors were
156 shown in supplement of Luo et al. (2022), and details about the determination of these factors are
157 introduced in supplement of Luo et al. (2022). Note that the AE33 measurements were only available
158 until 1th of November, while SP-AMS measurements were available until 18th of November, resulting
159 in different time frames of different timeseries.

160 Given that PMF analysis is fundamental to our study, the mass spectral profiles of factors are
161 provided in Fig. S1, and key aspects of the resolved results are explained here, particularly concerning
162 the O/C characteristics and the naming of aBBOA and Night-OA. In previous studies (Kuang et al.,
163 2021; Luo et al., 2022), we already realized that the correlation between aBBOA and $C_6H_2NO_4^+$ was
164 actually weak ($R=0.31$), suggesting that it might not fully be constituted of aging products of primary
165 BBOA considering its O/C was even lower than that of BBOA. However, aBBOA exhibited similar
166 diurnal behavior to LOOA showing clear daytime photochemical production plus an evening peak
167 around 19:00 (local time) just after the peak hour of BBOA as shown in Fig.S1. Also, the evening peak
168 value of aBBOA between 19:00 and 22:00 of each day was found to be moderately correlated with the
169 noon peak in the next day ($R=0.55$; (Wu et al., 2024)). This tells that aBBOA could be emitted from
170 biomass burning. However, it could be speculated that only a small portion (aBBOA accounts for an
171 average of 8% of the mass increase during identified biomass burning events, Fig. 3 of Luo et al.



172 (2022)) is directly emitted. Most of it likely originated from the gas-phase oxidation of biomass
173 burning emitted VOC precursors considering that aBBOA mainly added mass to diameters of
174 condensation mode (see discussions about size distributions of OA factors in supplement of Luo et al.
175 (2022)), which could have a low O/C during short oxidation periods, as demonstrated in previous
176 indoor experiments on biomass burning emissions (Yee et al., 2013; Ahern et al., 2019). This
177 hypothesis is further supported by the fact that increases in aBBOA loading enhance organic aerosol
178 hygroscopicity despite its low O/C, as demonstrated by Kuang et al. (2021), whereas primary organic
179 aerosols have not been observed to enhance overall organic aerosol hygroscopicity (Kuang et al., 2020).

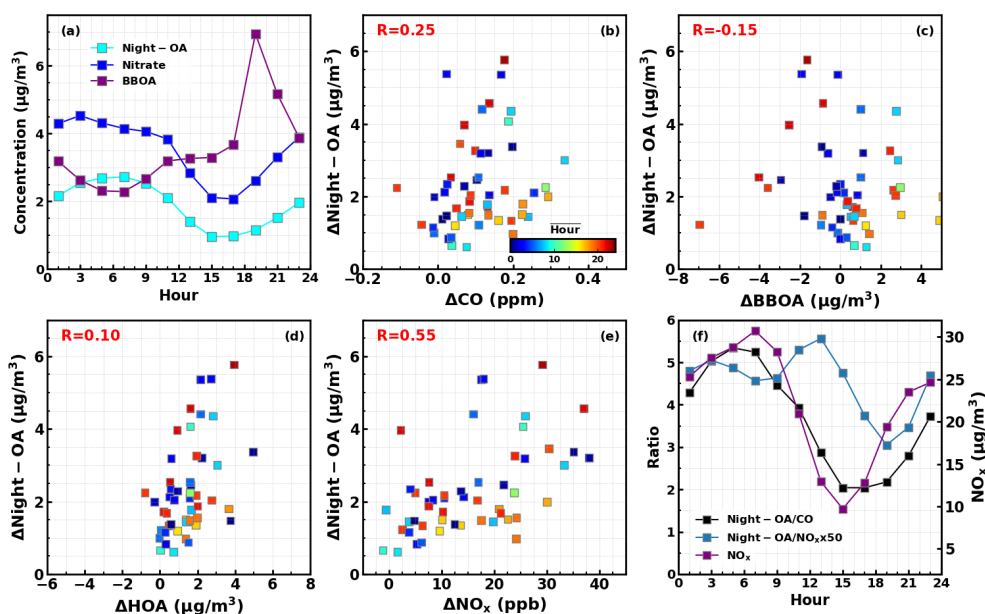


Figure 1. (a) Diurnal variations of nitrate, Night-OA and BBOA; (b-e) Relations between increases of Night-OA and increases of CO, BBOA, HOA and NO_x for identified Night-OA increase cases, colors of scatter plots represent the average time of Night-OA increase cases; (f) Diurnal variations of ratios Night-OA/CO, Night-OA/ NO_x in the left axis and NO_x in the right axis.

180 The Night-OA factor has a relatively low O/C ratio of 0.32, raising the question of whether it
181 originates from primary emissions or secondary formation. As discussed in Luo et al. (2022), traffic,
182 cooking (The HOA and COA and were not separated in the PMF results although the hydrocarbon
183 factor was named HOA as discussed in Kuang et al. (2021)), and biomass burning are likely the
184 dominant primary sources during this campaign. If Night-OA were a primary source, it would be
185 expected to increase alongside other primary sources. We identified most Night-OA increase events



186 and examined their correlation with variations in other primary sources, as shown in Fig. 1b-e. This
187 analysis reveals that Night-OA increases were typically observed after sunset, though occasionally
188 during the daytime. Night-OA increases showed weak correlations with changes of CO ($R=0.25$), HOA
189 ($R=0.1$), and BBOA ($R=-0.15$), but a moderate correlation with NO_x ($R=0.55$). During significant
190 biomass burning events (indicated by substantial BBOA increases), the concentration of Night-OA
191 actually decreased on average (Fig. 3 of Luo et al. (2022)), suggesting that Night-OA is unlikely to be
192 emitted from biomass burning. We also identified all significant HOA increase events that did not
193 coincide with biomass burning and analyzed the average HOA increase and variations in other aerosol
194 components (Fig. S2). It shows that, despite significant HOA increases, the average mass concentration
195 of Night-OA remained almost unchanged, indicating that Night-OA is also unlikely to originate from
196 HOA-associated emissions. Therefore, the weak but positive correlations between Night-OA and HOA
197 as well as CO are likely associated with the accumulation characteristics of primary emissions after
198 sunset. The higher correlations between Night-OA and NO_x may also result from the accumulation of
199 NO_x starting in the afternoon when photochemical depletion is weaker. Another possibility to consider
200 is whether Night-OA increases could be associated with plumes containing higher NO_x transported
201 from other regions. We investigated the diurnal variations of the Night-OA/CO and Night-OA/NO_x
202 ratios, observing persistent increases in Night-OA/CO and Night-OA/NO_x ratios when significant
203 Night-OA formation began. This suggests that Night-OA is likely formed through secondary processes,
204 consistent with that it was also correlated with nitrate ($R=0.67$). The low O/C of Night-OA, still higher
205 than that of the primary factor HOA, was determined by a high amount of C_xH_y⁺ ions in spite of
206 significant intensity of oxidation tracers C₂H₃O⁺ and CO₂⁺, suggesting that Night-OA was oxidation
207 products with low oxidation state during the nighttime. Similar situation was previously found in study
208 at Bakersfield of USA in which Liu et al. (2012) identified SOA factors as alkane-SOA and aromatic-
209 SOA with moderate O/C (0.27-0.36). Meanwhile, NO_x potentially promoted its formation, given the
210 highest N/C ratio of Night-OA among all resolved factors. This will be discussed further in Sect 3.2.

211 In summary, both aBBOA and Night-OA are not likely primary, while the naming of aBBOA and
212 Night-OA factors might not be perfect, we retain these terms in this study for consistency with our
213 previous work (Kuang et al., 2021; Luo et al., 2022; Wu et al., 2024).

214 **2.2 Quantification of BrC absorptions**

215 In Luo et al. (2022), we proposed an improved AAE ratio method to subtract brown carbon (BrC)



216 absorptions from measured total aerosol absorptions during this field campaign. Therefore, the details
217 about discussions of this method please refer to Luo et al. (2022), and we only introduce briefly the
218 philosophy of the new method here. The essential part of deconvolving BrC absorptions from total
219 aerosol absorptions is the adequate representation of black carbon (BC) spectral absorptions using the
220 Ångström exponent law. Results of previous studies (Wang et al., 2018a; Li et al., 2019a) demonstrated
221 that significant wavelength dependence of AAE_{BC} and constant assumption of AAE_{BC} in BrC
222 absorption retrievals might lead to significant bias. Thus, the AAE ratio defined as
223 $R_{AAE}(\lambda) = AAE_{BC, \lambda-880} / AAE_{BC, 950-880}$ was proposed to tackle spectral AAE_{BC} variations, and on-line
224 measurement data of $AAE_{950-880}$ were used as $AAE_{BC, 950-880}$ due to negligible absorption
225 contributions of BrC at wavelengths of 880 nm and 950 nm. Thus, BrC absorptions (σ_{BrC}) at different
226 wavelength (λ) including 370 nm, 470 nm, 530 nm, 590 nm and 660 nm can be derived using the
227 following formula, where σ_a is measured aerosol absorption:

$$228 \quad \sigma_{BrC}(\lambda) = \sigma_a(\lambda) - \sigma_{BC}(880 \text{ nm}) \times \left(\frac{880}{\lambda}\right)^{AAE_{BC, 950-880} \times R_{AAE}(\lambda)} \quad (1)$$

229 As the sophisticated discussions presented in Luo et al. (2022), variations of many factors such
230 as BC refractive index, coating shell refractive index as well as BC mixing state, and BC mass size
231 distributions (Li et al., 2019b) might influences the magnitudes of $R_{AAE}(\lambda)$. However, sensitivity tests
232 shown in Luo et al. (2022) clearly concluded that BC mass size distributions dominated $R_{AAE}(\lambda)$
233 variations. In Heshan campaign, the BC calibration for SP-AMS was not available, so, the carbon
234 signals were used to retrieve shape of BC mass size distribution, and the total mass was constrained
235 by the ratio between integrated C_x (C_1 - C_9) signals and BC mass concentrations provided by the AE33.
236 The real-time measured carbon fragments (C_x) distributions by the SP-AMS were therefore used to
237 distribute the total BC mass to different diameter bins to calculate $R_{AAE}(\lambda)$ as introduced in Luo et al.
238 (2022). Details of the calculation can be found in its supplement. The average and standard deviations
239 of $R_{AAE}(370)$, $R_{AAE}(470)$, $R_{AAE}(520)$, $R_{AAE}(590)$ and $R_{AAE}(660)$ are $0.79(\pm 0.044)$, $0.85(\pm 0.038)$,
240 $0.88(\pm 0.035)$, $0.9(\pm 0.035)$ and $0.93(\pm 0.031)$ during the observation period.

241 **3 Results and discussions**

242 **3.1 Highly absorptive SOA formed during nighttime.**

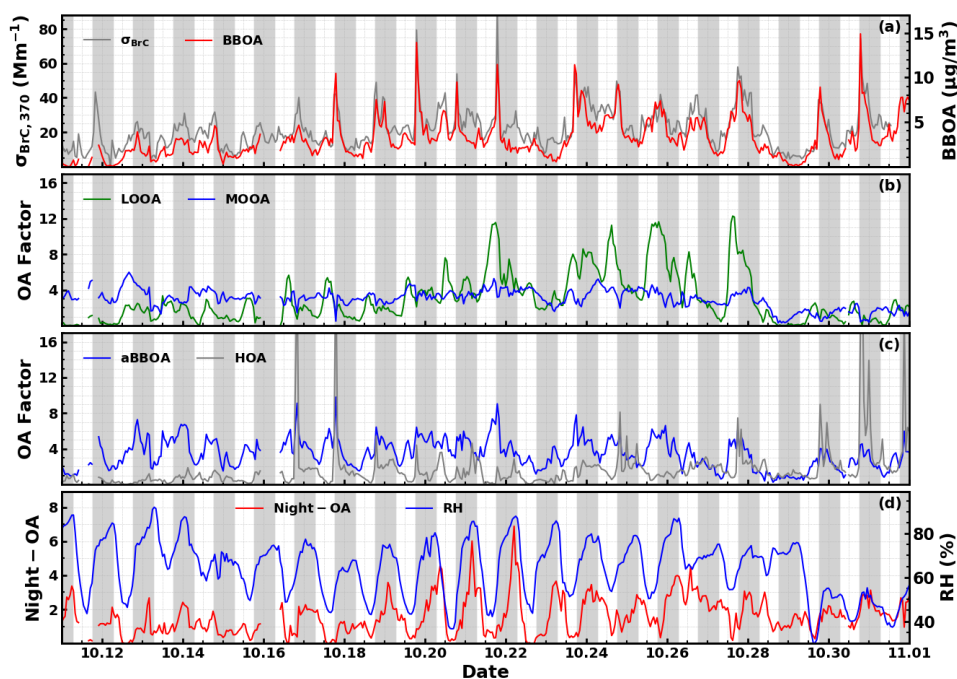


Figure 2. Timeseries of (a) brown carbon absorption at 370 nm ($\sigma_{BrC,370}$) in the left axis and BBOA in the right axis; (b) LOOA and MOOA; (c) aBBOA and HOA; (d) Night-OA in the left axis and RH in the right axis. Shaded areas represent nighttime periods.

243 As reported by Luo et al. (2022), biomass burning events happened frequently during the
244 observation period and biomass burning was the dominant source of primary organic aerosols with the
245 average BBOA/HOA ratio of 3.3. The dominant contribution of biomass burning to primary aerosol
246 emissions together with the strong biomass burning emissions before dusk as well as sometimes
247 daytime emission characteristics (Luo et al., 2022) provided a unique opportunity to explore the
248 nighttime chemistry associated with biomass burning and its impacts on atmospheric BrC evolution in
249 biomass burning plumes. Timeseries of retrieved $\sigma_{BrC,370}$ is shown in Fig.2a. It shows that BBOA
250 varies quite consistently with $\sigma_{BrC,370}$ and they are highly correlated ($R=0.88$), demonstrating the
251 dominant contribution of BBOA to BrC absorptions. However, the correlation coefficient between
252 BBOA and σ_{BrC} decreases as the wavelength increases, i.e., the correlation coefficients between σ_{BrC}
253 at 470 nm, 520 nm, 590 nm, 660 nm and BBOA are 0.83, 0.8, 0.76, 0.69. In addition, as shown in
254 Fig.2a, coordinational variations between BBOA $\sigma_{BrC,370}$ are usually seen during daytime especially during
255 the dusk BBOA spike periods, however, the $\sigma_{BrC,370}$ usually deviates substantially from BBOA



256 variations during the nighttime (gray areas in Fig.2). The average diurnal variations of both $\sigma_{BrC,370}$
257 and the ratio $\sigma_{BrC,370}/BBOA$ is presented in Fig.3a, and quick $\sigma_{BrC,370}/BBOA$ increase were observed
258 during nighttime before 06:00 LT. These results demonstrate that organic aerosol components other
259 than BBOA also contribute substantially to BrC absorption and differ much at different wavelengths.

260 The time series of OA factors other than BBOA are also shown in Fig.2b-d. As analyzed in Kuang
261 et al. (2021), SOA contribute dominantly to total OA mass (SOA mass fraction >70% on average)
262 during this field campaign. Most prominent features of SOA formations are the quick daytime
263 formation of LOOA, aBBOA and nighttime formation of Night-OA, while MOOA exhibit almost no
264 diurnal variations and are mostly associated with the regional airmass. The average mass absorption
265 efficiencies (MAEs) (m^2/g) of different OA factors are retrieved using multivariate linear regression
266 method (Fig.S3), and the deduced average MAEs values at 370 nm for BBOA, aBBOA, HOA, LOOA,
267 MOOA and Night-OA are 3.8, 0.84, 0.24, 0, 1, 2.3 m^2/g respectively. Note that negative value of about
268 -0.1 is retrieved if LOOA values were inputs of the multivariate linear regressions, demonstrating quite
269 low absorptivity of LOOA, thus MAE of LOOA is treated as zero. As shown in Fig.2b, rapid LOOA
270 formation episodes happened frequently during daytime but $\sigma_{BrC,370}$ still varies only with BBOA
271 during that period, which confirms the white property of LOOA. The derived MAE of HOA is very
272 small which is consistent with the low absorptivity of HOA during HOA spikes. The prominent BrC
273 factors are identified as BBOA, Night-OA, MOOA and aBBOA. The most surprising part is the highly
274 absorptive property of Night-OA whose absorptivity is only lower than that of BBOA but much higher
275 than other OA factors. Based on derived MAE values for OA factors as well as their mass
276 concentrations, contributions of OA factors to $\sigma_{BrC,370}$ are estimated and their diurnal variations are
277 shown in Fig.3b. It reveals that Night-OA accounts for the second largest contribution to BrC
278 absorption during nighttime and even reaches beyond the contribution of BBOA near local time 06:00
279 (>30%), which explains the observed substantial nighttime deviation of $\sigma_{BrC,370}$ from BBOA as shown
280 in Fig.3a. The average contributions of BBOA, Night-OA, MOOA and aBBOA to $\sigma_{BrC,370}$ are 50%,
281 20%, 16%, 12%, respectively. The time series of estimated OA contributions to BrC absorption at 370
282 nm are shown in Fig.S4, it tells that Night-OA sometimes contribute dominantly (>50%) to $\sigma_{BrC,370}$
283 especially when rapid increase of Night-OA appeared due to nighttime secondary formation.

284 Different BrC components usually exhibit different absorption spectral dependences (Laskin et
285 al., 2015). Diurnal variations of $AAE_{370-470, BrC}$ are investigated and shown in Fig.3c. The $AAE_{370-470}$,

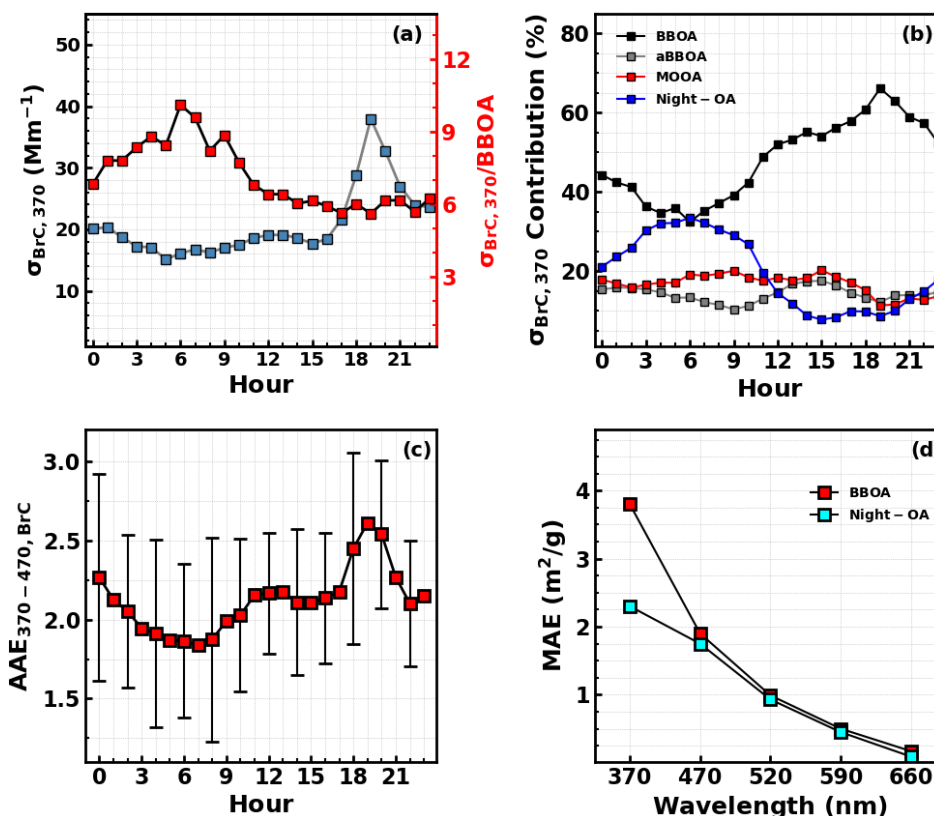


Figure 3. (a) Diurnal variations of $\sigma_{BrC,370}$ and the ratio $\sigma_{BrC,370}/BBOA$; (b) Diurnal variations of contributions of different OA factors to $\sigma_{BrC,370}$; (c) Average diurnal variations of brown carbon absorption angstrom exponent between 370 nm and 470 nm; (d) Retrieved mass absorption efficiencies (MAE,) of BBOA and Night-OA at multi-wavelengths.

286 σ_{BrC} exhibits distinct diurnal variations, with one peak at dusk when BBOA reaches its highest mass
 287 concentration and a trough at the time when Night-OA contributes most to and BBOA contribute the
 288 least to $\sigma_{BrC,370}$. This phenomenon suggests that spectral dependence of Night-OA absorptivity differs
 289 much with that of BBOA. The multivariate linear regression method is thus also used for retrieving
 290 MAEs of BBOA and Night-OA at wavelengths of 470 nm, 520 nm, 590 nm and 660 nm (the
 291 performance of using retrieved MAE values at multiple wavelengths are shown in Fig.S3), and the
 292 retrieved spectral dependence of BBOA and Night-OA absorptivity are shown in Fig.3d. The results
 293 show that Night-OA absorbs as strong as that of BBOA at visible wavelength ranges, highlighting a
 294 more important role of Night-OA in BrC absorption than expected from the retrieval of $\sigma_{BrC,370}$. The



295 retrieved $AAE_{370-470}$, $AAE_{470-590}$ for BBOA and Night-OA are 3 and 5.9, 1.3 and 6, respectively, which
296 explains the observed quick decrease of $AAE_{370-470, BrC}$ during nighttime. The direct quantification of
297 $AAE_{370-470}$, $AAE_{470-590}$ for BBOA is difficult due to the entanglement of BC absorption and thus rarely
298 reported. The retrieved $AAE_{470-590}$ for BBOA and Night OA are in general consistent with the AAE of
299 bulk BrC solutions extracted using different solvents which were sampled during and after a nighttime
300 nationwide biomass burning event (Lin et al., 2017).

301 **3.2 Precursors and Possible Mechanisms of the Night-OA formation.**

302 As shown in Fig.1a and Fig.2d, the Night-OA concentration increased during the nighttime, while
303 usually decreased and reached near zero in the afternoon, so the Night-OA factor is characterized by
304 its rapid nighttime formation and quick daytime evaporation. In general, SOA can either be formed
305 through condensation of gas-phase chemically aged low- or semi-volatile VOC precursors following
306 the gas-particle partitioning theory or formed in the aqueous phase through further oxidation of water-
307 soluble primary VOCs as well as secondary products of gas-phase VOC aging processes, with the
308 former referred to as gasSOA and the latter referred to as aqSOA. Several recent researches reveal that
309 SOA can also be formed through oxidation of semi-volatile components evaporated from emitted
310 primary organic aerosols in gas phase (Palm et al., 2020) or in the aqueous phase (Wang et al., 2021).
311 The sources and formation pathways of Night-OA is of great concern in meriting the importance of
312 Night-OA formations in global atmosphere and paving the way for designing targeted laboratory
313 experiments in future.

314 The VOC profiles of this observation site are quite complex as mixtures of both different
315 anthropogenic sources and natural sources (Song et al., 2019). However, prominent and continuous
316 Night-OA formation events observed from 19 to 22 October which are accompanied with frequently
317 observed sharp increase of BBOA mass concentrations before the fall of night bring hints that Night-
318 OA formation might be associated with biomass burning emissions. Indeed, the air is always moving
319 and to be lagrangian, the air after midnight might differ with those before midnight. However, the
320 relations between Night-OA signals after midnight and emission signals before midnight might still
321 deliver some clues. The average nighttime mass concentrations of Night-OA from 22:00 LT to 06:00
322 LT (the next day) are plotted against the average BBOA mass concentrations from 16:00 LT to 22:00
323 LT of this campaign and the results are shown in Fig.4a. It shows that Night-OA formation is positively
324 correlated with BBOA before the night which supports the speculation that Night-OA formation is a



325 result of the nighttime chemistry of biomass burning emissions. The nighttime oxidant levels indicated
 326 by the concentrations of Ox ($\text{NO}_2 + \text{O}_3$) represented by colors in Fig.4a demonstrates that the highest
 327 Night-OA formation was accompanied with strongest biomass burning emissions and most abundant
 328 oxidants, suggesting that the importance of nighttime aging processes in Night-OA formation.
 329 Following evidences show that gas-phase and aqueous-phase chemistry of biomass burning precursors
 330 likely have coordinated to promote the quick nighttime formation of Night-OA.

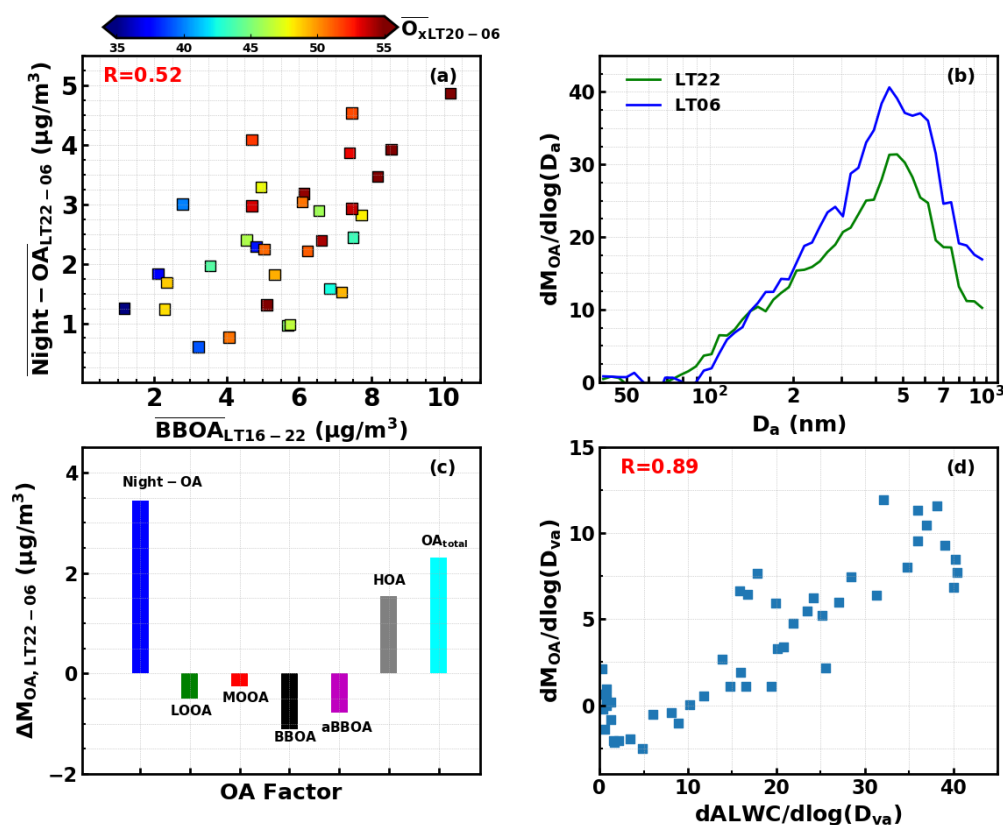


Figure 4. (a) Correlations between average nighttime Night-OA mass concentrations and average BBOA mass concentrations over LT16-22, colors corresponding to the average Ox ($\text{NO}_2 + \text{O}_3$) mixing ratio (ppb) during the night; (b) Average evolutions of organic aerosol mass size distributions from local time 22:00 (20, 21 October) to 06:00 (21, 22 October); (c) Average differences for organic aerosol (OA) mass concentration corresponding to (b); (d) The correlations between increase of size-resolved organic mass concentrations in (c) (LT06 minus LT22) with average size-resolved aerosol liquid water content (ALWC).

331 Three obvious Night-OA formation episodes which lasted more than three days, as shown in
 332 Fig.S5, were observed during the entire field campaign. The peak Night-OA mass concentration of



333 each night increased during these episodes and were accompanied with the increase of nighttime peak
334 RH during each episode, suggesting that abundant nighttime aerosol water might play significant roles
335 in Night-OA formation. More solid clues could be found from different behaviors of gasSOA and
336 aqSOA formations in modifying the aerosol size distribution. The gasSOA forms through condensation
337 following partitioning theory thus adding mass mainly to condensation mode which contributes most
338 to aerosol surface area concentrations. Whereas, aqSOA formation depends on amounts of liquid water
339 content thus adding mass mainly to the mode where most aerosol water resides. The evolution of
340 average OA size distribution during the night of 20 and 21 October when most prominent Night-OA
341 formation occurred is illustrated in Fig.4b. During the two nights from 22:00 LT to 06:00 LT, Night-
342 OA formations contributed most to the mass concentration increase of the entire OA and HOA
343 contributed less, while mass concentrations of all other OA factors have decreased and partially
344 balanced out the OA increase (Fig.4c). HOA emissions mainly added mass to diameter ranges of 100-
345 300 nm as demonstrated by Luo et al. (2022). However, as shown in Fig.4b, substantial increase of
346 mass concentrations at diameter range of > 300 nm occurred even all other SOA factors showed a
347 decreasing trend for the case shown in Fig.4c, suggesting the substantial OA mass increase of larger
348 than 300 nm are contributed by the Night-OA increase. The results shown in Fig.4d showed that the
349 size-resolved increase of OA mass for abovementioned cases (Fig.4b and c) was highly correlated with
350 size-resolved aerosol liquid water content (details about the size resolved aerosol water content
351 calculation are presented in Sect 1.2 of the supplement), demonstrating that the Night-OA formation
352 added mass mainly to aerosol water abundant diameter ranges. The average RH of the cases shown in
353 Fig.4b-d is around 80%, with a corresponding average hygroscopicity parameter κ of 0.26 measured
354 by the humidified nephelometer system, demonstrating a growth factor of ~ 1.27 (water thickness of
355 ~ 81 nm for aerosol diameter of about 300 nm), thus not a thin film of water for heterogeneous reactions,
356 but more likely formed through dark aqueous reactions.

357 In addition, as shown in Fig.S6, the Night-OA decreased quickly during daytime, which is beyond
358 the dilution effect of boundary layer development (indicated by rapid decrease of Night-OA/CO as
359 shown in Fig.S6) thus implying the substantial daytime loss of Night-OA which might be caused by
360 several processes, such as partitioning and photodegradation (Wang et al., 2023). The partitioning
361 dynamics of gasSOA and aqSOA also differ much, which might add more information in looking into
362 the Night-OA formation pathway. Following the rule of partitioning theory, evaporation equilibrium



363 of the condensation of gasSOA is tightly associated with air temperature. Equilibrium of the reversible
364 aqSOA formation greatly depends on aerosol water changes, while evaporation of irreversible SOA
365 production through aqueous pathways are quite sophisticated (Tong et al., 2021). It was found that the
366 percentile of Night-OA mass loss during the daytime (07:00 to 16:00 LT) are more tightly correlated
367 with RH decrease compared with temperature increase (Fig.S7). HOA also exhibits obvious
368 evaporation during daytime (indicated by rapid decrease of HOA/CO Fig.S6), however, the daytime
369 loss of HOA seems more tightly correlated with temperature increase as shown in Fig.S8. The
370 phenomenon that Night-OA daytime loss is more correlated with RH decrease implied that Night-OA
371 possibly co-evaporated with water vapor as RH decrease. This might serve weakly but still another
372 supporting clue for that Night-OA were likely formed through aqueous pathways and maybe reversible.

373 As revealed by Fig.4a that nighttime oxidation levels play significant roles in Night-OA formation,
374 the question leaves what's the role of nighttime gas-phase chemistry in promoting the Night-OA
375 formation.

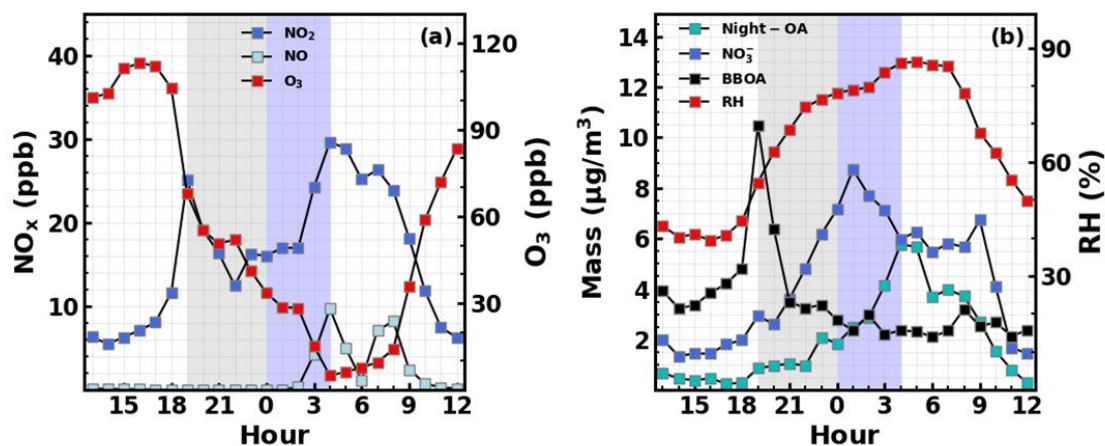


Figure 5. Average diurnal variations of (a) NO₂, NO, O₃; (b) Night-OA, nitrate, BBOA and RH during the two nights: 20 to 21 October when most prominent Night-OA formation occurred. Shaded areas represent periods of Night-OA increased, and blue parts correspond to remarkable increase period of Night-OA.

376 The average diurnal variations of gas pollutants and meteorological parameters typical of
377 nighttime chemistry including NO, NO₂, O₃, Night-OA, nitrate, RH as well as BBOA for the most
378 prominent Night-OA formation case (20 to 21, October, consistent with Fig.4b) are shown in Fig.5. At
379 at night, NO₂ and NO₃ radical do not photolyze, NO reacts rapidly with O₃ and as a result almost all NO_x



380 is concerted to NO_2 (Fig.5a). NO_2 will further react with O_3 to form NO_3 radical which is the most
381 important gas-phase oxidant during the nighttime (Chapleski et al., 2016). In this case, NO_2
382 concentration increased substantially before the sunset but the trend ended and shifted suddenly to
383 decrease when BBOA emissions were highest and then decreased rapidly along with the dropping
384 BBOA mass concentration. The reduction of BBOA mass concentration mainly attributed to the end
385 of local combustion events might also be associated with BBOA evaporation after its strong emissions
386 due to the mix of biomass burning plumes with background airmass, and this dilution effects shall
387 deliver semi-volatile VOCs such as phenolic compounds from particle phase to gas phase (Palm et al.,
388 2020). The Night-OA increased slowly during the rapid NO_2 decrease phase but nitrate concentration
389 increased substantially with decreasing O_3 concentration (still higher than 30 ppb as shown in gray
390 shaded areas). The hydrolysis of N_2O_5 , which is formed from NO_2 addition of NO_3 radicals, represents
391 an important pathway of nitrate formation during nighttime period. The rapid decrease of NO_2
392 coincident with the quick nitrate formation implies that the rapid NO_2 consumption supplied the NO_3
393 and N_2O_5 reaction chains, providing abundant NO_3 radical during the initial stage of Night-OA
394 formation. The active nighttime NO_3 chemistry and its impacts on nitrate formations during the
395 observation periods were further confirmed by Yang et al. (2022) who conducted box model
396 simulations. In addition, Li, et al. (2020a) demonstrated that night NO_3 radical darkened the BBOA
397 with the MAE enhancement ratio range from 1.3 to 3.2 for optical wavelength of less than 650 nm.
398 The retrieved average MAE of BBOA through multilinear fitting was higher than the average MAE of
399 freshly emitted BBOA during BBOA spikes as reported by Luo et al. (2022) (3.8 vs 2.6 m^2/g),
400 suggesting the darkening of primary BBOA which is consistent with the prevailing nighttime NO_3
401 chemistry processes during the observations. The highest Night-OA production rate occurred when
402 both NO_2 and NO began to increase (O_3 still decreased rapidly and reached below 30 ppb, shown as
403 the blue shaded area) and the RH reached near the its maximum, which further highlights the crucial
404 role of aerosol liquid water content in Night-OA formation. However, the quick increase of NO_2 and
405 NO implies that the dominant contribution of NO_2 formation to O_3 depletion, and the NO_3 radical
406 chemistry have ceased and likely did not directly participate in the succeeding quick aqueous-phase
407 Night-OA formation. Nevertheless, quick depletion of O_3 and increase of NO_2 with the quickest Night-
408 OA formation occurred demonstrates that the NO_2 might play significant roles in the subsequent quick
409 Night-OA formation. These results demonstrate that the aqueous-phase processing of biomass burning



410 emissions with abundant NO_2 could likely form highly absorptive SOA, while the nighttime gas-phase
411 chemistry with typically high NO_2 , NO_3 radical and RH could likely magnify the Night-OA formation.
412 A previous field study (Lin et al., 2017) demonstrated that most chromophores were nitroaromatic
413 compounds (NAC) during the observed nighttime bonfire event with the major contribution to the
414 solvent extractable BrC, and the NAC contribution to BrC absorption increased towards near visible
415 wavelengths, and this characteristics is consistent with the aforementioned BrC absorption spectral
416 dependence characteristics in Sect 3.1. Actually, the relatively low O/C of Night-OA while high N/C
417 and H/C ratios (0.04 and 1.89, even higher than those of BBOA which are known composed of complex
418 nitrogen containing compounds) was consistent with the features (low O/C, high N/C (ring- and N-
419 containing structures of NACs) and low hygroscopicity) of aerosols that involved such as nitro-
420 phenolic compounds (Chen et al., 2022) secondarily formed from reactions of cyclic aromatics that
421 involve NO_3 radical chemistry (Rana and Guzman, 2022; Mayorga et al., 2021) during nighttime which
422 likely have larger molecular weight and thereby lower hygroscopicity (Wang et al., 2019a; Price et al.,
423 2022; Petters et al., 2009). The increased loading of Night-OA would lower organic aerosol
424 hygroscopicity, which was confirmed previously by Kuang et al. (2021). However, the high N/C of
425 Night-OA was consistent with its strong absorptivity considering that aerosol absorptions are generally
426 linked with N-containing components (Qin et al., 2018; Kasthuriarachchi et al., 2020), however, N/C
427 of 0.04 implies the complex structures of Night-OA components. These results also demonstrate that
428 NAC are probably key components of the Night-OA factor, considering that biomass burning was
429 indeed important sources of precursors (Li et al., 2020b; Decker et al., 2019) to form NACs, consistent
430 with the inference that precursors of Night-OA came from biomass burning. On the basis of limited
431 existing literatures, Wang et al. (2019c) have summarized the secondary NAC formation pathways of
432 benzene, toluene, phenol and methylcatechol which represented a significant fraction of biomass
433 burning VOC emissions (Stockwell et al., 2015), and emphasized that the NO_3 radical does not directly
434 participate in the aqueous phase reactions in NAC formation reaction chains, but first oxidizes these
435 precursors into intermediate products which then react with NO_2 to form nitrophenols and
436 nitrocatechols that are further oxidized in the particle phase to generate NAC. This gas-phase oxidation
437 and subsequent particle-phase reaction chains of NAC production may explain the observed Night-OA
438 formation characteristics that the most-prominent Night-OA formation occurred after the strongest
439 NO_3 radical chemistry when the aerosol liquid water content was abundant, highlighting the great



440 importance of nighttime multiphase chemistry in Night-OA formation. Aside from the case shown in
441 Fig.5, much higher correlation coefficient between nighttime average Night-OA mass concentration
442 and nighttime average O_x concentrations than that of NO_2 shown in Fig.S9 for the entire campaign
443 (0.58 versus 0.39) further stresses that the coordination of night-time gas-phase and aqueous-phase
444 was responsible for the quick Night-OA formation. In addition, obvious daytime increase in Night-OA
445 was occasionally observed (Fig.S10 and Fig.S11) as mentioned in Sect.2 when the RH remain high
446 and NO_2 as well as biomass burning emissions increased substantially. This results further emphasizes
447 that NO_2 might play significant roles in aqueous phase reactions of oxidized biomass burning
448 precursors which might be directly emitted or transformed through active nighttime NO_3 chemistry
449 (Decker et al., 2019).

450

451 **4. Environmental and climate significance**

452 Biomass burning emissions, as the largest sources of primary aerosols and the second largest
453 sources of VOCs, exert increasingly greater impacts on the regional air quality and global climate
454 under the context of global warming (Running, 2006). However, the lack of knowledge on the complex
455 chemical aging of biomass burning plumes during its transport hinders the accurate representation of
456 biomass burning VOCs and BBOA evolution in air quality and climate models. Kodros et al. (2022)
457 concluded based on laboratory experiments that dark aging of biomass burning emissions was sensitive
458 to RH, and their results suggested that the SOA was mainly formed through condensation of gas-phase
459 oxidation products, however, not ruling out the possibility of heterogeneous oxidations. This study
460 highlights that nighttime gas-phase chemistry of biomass burning VOC precursors in conjunction with
461 further aqueous-phase reactions likely contributed substantially to ambient SOA that is highly
462 absorptive. Although more comprehensive studies about detailed mechanisms are needed and the
463 robustness of the conclusion in this study needs to be further examined as well as the exact types of
464 fires during this campaign are not known, still, this finding has important implications for our
465 understanding on nighttime evolution of biomass burning plumes. Field observations in this study
466 revealed the abundant existence of highly hygroscopic inorganic components within ambient aerosols
467 that contributed substantially to aerosol liquid water in ambient air, while aerosols produced in the
468 chamber of Kodros et al. (2022) were dominated by organics (only with very small amounts of
469 inorganic nitrate formed during the aging processes) which might have inhibited aqueous reaction



470 pathways. Inspired by this study, future laboratory studies investigating nighttime aging of biomass
471 burning plumes should consider not only the high nighttime RH conditions, but also the complex
472 mixture of background inorganic aerosols with biomass burning emissions when simulating aerosols
473 within biomass burning plumes.

474 In addition, biomass burning plumes might form convective clouds under strong ground surface
475 heating and moisture release (pyrocumulus clouds or pyrocumulonimbus clouds) (Andreae et al.,
476 2004;Fromm et al., 2006;Cunningham and Reeder, 2009;Lareau and Clements, 2016), or interact with
477 clouds/fogs during long-range transport (Engelhart et al., 2011). Clouds/fogs provide large amount of
478 liquid water regardless of day or night, while active photochemistry in biomass burning plumes may
479 increase O₃ and NO₂ production (Hecobian et al., 2011;Marufu et al., 2000;Ziemke et al., 2009)
480 (biomass burning also emits NO₂ directly as shown in Fig.45, likely promoting NO₃ radical production
481 (Selimovic et al., 2020) during nighttime. This suggests a potential formation of highly absorptive
482 SOA in cloud droplets, which results in even browner cloud droplets, impacting cloud optical
483 properties, cloud lifetime (e.g. promoting cloud burning off effect) and precipitation. Especially, since
484 violent pyroconvection can penetrate into the stratosphere, darkening of clouds might have regional
485 impacts on cloud properties as well as radiative balance. Moreover, the biomass burning plumes
486 transported from remote areas can sometimes mix down into the boundary layer and exert significant
487 impacts on regional air quality (Wang et al., 2018b). The top of the boundary layer is usually
488 characterized by high RH conditions due to abundant water vapor but lower temperatures, as well as
489 high O_x concentrations due to substantial anthropogenic NO_x emissions and active photochemistry,
490 and thus potentially large amounts of highly absorptive SOA formation could be expected in this kind
491 of biomass burning plumes.

492 Overall, results of this study provide important insights into nighttime evolutions of biomass
493 burning and an uncovered potential secondary BrC formation mechanism that has broad implications
494 for climate and air quality effects of biomass burning, especially the interaction between biomass
495 burning plumes with clouds in the aging process during nighttime. However, much more efforts are
496 still required to further disentangle the complex routes of gas-phase biomass burning VOC oxidation
497 and subsequent aqueous-phase reactions.

498
499



500 **Data availability.** The data used in this study are available from the corresponding author upon
501 request Ye Kuang (kuangye@jnu.edu.cn) and Shan Huang (shanhuang_eci@jnu.edu.cn)

502 **Competing interests.** The authors declare no competing financial interest.
503

504 **Author Contributions.** YK conceived this research and wrote the manuscript. SH conducted the
505 SPAMS measurements and performed the PMF analysis. BL performed the AE33 measurements. MS
506 and BY planned this campaign. JL, WH, YP, DC, and DY participated this campaign and provided
507 full support for the campaign. WX provided insights into reaction mechanism analysis.
508

509 **Financial supports.** This work is supported by the National Natural Science Foundation of China
510 (grant No. 41805109, 41807302), National Key Research and Development Program of China (grant
511 No. 2017YFC0212803, 2016YFC0202206), Key-Area Research and Development Program of
512 Guangdong Province (grant No. 2019B110206001), Special Fund Project for Science and Technology
513 Innovation Strategy of Guangdong Province (grant No.2019B121205004), Guangdong Natural
514 Science Funds for Distinguished Young Scholar (grant No. 2018B030306037).

515

516

517

518

519

520

521

522

523

524



525 References

- 526 Akagi, S. K., Yokelson, R. J., Wiedinmyer, C., Alvarado, M. J., Reid, J. S., Karl, T., Crouse, J. D., and Wennberg, P. O.: Emission
527 factors for open and domestic biomass burning for use in atmospheric models, *Atmos. Chem. Phys.*, 11, 4039-4072,
528 10.5194/acp-11-4039-2011, 2011.
- 529 Andreae, M. O., and Merlet, P.: Emission of trace gases and aerosols from biomass burning, *Global Biogeochemical Cycles*,
530 15, 955-966, <https://doi.org/10.1029/2000GB001382>, 2001.
- 531 Andreae, M. O., Rosenfeld, D., Artaxo, P., Costa, A. A., Frank, G. P., Longo, K. M., and Silva-Dias, M. A. F.: Smoking Rain
532 Clouds over the Amazon, *Science*, 303, 1337-1342, doi:10.1126/science.1092779, 2004.
- 533 Andreae, M. O., and Gelencsér, A.: Black carbon or brown carbon? The nature of light-absorbing carbonaceous aerosols,
534 *Atmos. Chem. Phys.*, 6, 3131-3148, 10.5194/acp-6-3131-2006, 2006.
- 535 Andreae, M. O.: Emission of trace gases and aerosols from biomass burning – an updated assessment, *Atmos. Chem. Phys.*,
536 19, 8523-8546, 10.5194/acp-19-8523-2019, 2019.
- 537 Bertrand, A., Stefenelli, G., Jen, C. N., Pieber, S. M., Bruns, E. A., Ni, H., Temime-Roussel, B., Slowik, J. G., Goldstein, A. H.,
538 El Haddad, I., Baltensperger, U., Prévôt, A. S. H., Wortham, H., and Marchand, N.: Evolution of the chemical fingerprint of
539 biomass burning organic aerosol during aging, *Atmospheric Chemistry and Physics*, 18, 7607-7624, 10.5194/acp-18-7607-
540 2018, 2018.
- 541 Bluvshstein, N., Lin, P., Flores, J. M., Segev, L., Mazar, Y., Tas, E., Snider, G., Weagle, C., Brown, S. S., Laskin, A., and Rudich,
542 Y.: Broadband optical properties of biomass-burning aerosol and identification of brown carbon chromophores, *Journal*
543 *of Geophysical Research: Atmospheres*, 122, 5441-5456, <https://doi.org/10.1002/2016JD026230>, 2017.
- 544 Chapleski, R. C., Zhang, Y., Troya, D., and Morris, J. R.: Heterogeneous chemistry and reaction dynamics of the atmospheric
545 oxidants, O₃, NO₃, and OH, on organic surfaces, *Chem Soc Rev*, 45, 3731-3746, 10.1039/c5cs00375j, 2016.
- 546 Chen, Y., Zheng, P., Wang, Z., Pu, W., Tan, Y., Yu, C., Xia, M., Wang, W., Guo, J., Huang, D., Yan, C., Nie, W., Ling, Z., Chen,
547 Q., Lee, S., and Wang, T.: Secondary Formation and Impacts of Gaseous Nitro-Phenolic Compounds in the Continental
548 Outflow Observed at a Background Site in South China, *Environmental science & technology*, 56, 6933-6943,
549 10.1021/acs.est.1c04596, 2022.
- 550 Cheng, Z., Atwi, K. M., Yu, Z., Avery, A., Fortner, E. C., Williams, L., Majluf, F., Krechmer, J. E., Lambe, A. T., and Saleh, R.:
551 Evolution of the light-absorption properties of combustion brown carbon aerosols following reaction with nitrate radicals,
552 *Aerosol Science and Technology*, 1-15, 10.1080/02786826.2020.1726867, 2020.
- 553 Cunningham, P., and Reeder, M. J.: Severe convective storms initiated by intense wildfires: Numerical simulations of pyro-
554 convection and pyro-tornadogenesis, *Geophysical Research Letters*, 36, <https://doi.org/10.1029/2009GL039262>, 2009.
- 555 Decker, Z. C. J., Zarzana, K. J., Coggon, M., Min, K.-E., Pollack, I., Ryerson, T. B., Peischl, J., Edwards, P., Dubé, W. P., Markovic,
556 M. Z., Roberts, J. M., Veres, P. R., Graus, M., Warneke, C., de Gouw, J., Hatch, L. E., Barsanti, K. C., and Brown, S. S.:
557 Nighttime Chemical Transformation in Biomass Burning Plumes: A Box Model Analysis Initialized with Aircraft
558 Observations, *Environmental science & technology*, 53, 2529-2538, 10.1021/acs.est.8b05359, 2019.
- 559 Drinovec, L., Močnik, G., Zotter, P., Prévôt, A. S. H., Ruckstuhl, C., Coz, E., Rupakheti, M., Sciare, J., Müller, T., Wiedensohler,
560 A., and Hansen, A. D. A.: The "dual-spot" Aethalometer: an improved measurement of aerosol black carbon with real-
561 time loading compensation, *Atmospheric Measurement Techniques*, 8, 1965-1979, 10.5194/amt-8-1965-2015, 2015.



- 562 Engelhart, G. J., Moore, R. H., Nenes, A., and Pandis, S. N.: Cloud condensation nuclei activity of isoprene secondary
563 organic aerosol, *Journal of Geophysical Research: Atmospheres*, 116, 10.1029/2010jd014706, 2011.
- 564 Fromm, M., Tupper, A., Rosenfeld, D., Servranckx, R., and McRae, R.: Violent pyro-convective storm devastates Australia's
565 capital and pollutes the stratosphere, *Geophysical Research Letters*, 33, <https://doi.org/10.1029/2005GL025161>, 2006.
- 566 Hartikainen, A., Yli-Pirilä, P., Tiitta, P., Leskinen, A., Kortelainen, M., Orasche, J., Schnelle-Kreis, J., Lehtinen, K. E. J.,
567 Zimmermann, R., Jokiniemi, J., and Sippula, O.: Volatile Organic Compounds from Logwood Combustion: Emissions and
568 Transformation under Dark and Photochemical Aging Conditions in a Smog Chamber, *Environmental science & technology*,
569 52, 4979-4988, 10.1021/acs.est.7b06269, 2018.
- 570 Hecobian, A., Liu, Z., Hennigan, C. J., Huey, L. G., Jimenez, J. L., Cubison, M. J., Vay, S., Diskin, G. S., Sachse, G. W., Wisthaler,
571 A., Mikoviny, T., Weinheimer, A. J., Liao, J., Knapp, D. J., Wennberg, P. O., Kürten, A., Crounse, J. D., Clair, J. S., Wang, Y., and
572 Weber, R. J.: Comparison of chemical characteristics of 495 biomass burning plumes intercepted by the NASA DC-8 aircraft
573 during the ARCTAS/CARB-2008 field campaign, *Atmos. Chem. Phys.*, 11, 13325-13337, 10.5194/acp-11-13325-2011, 2011.
- 574 Hodshire, A. L., Akherati, A., Alvarado, M. J., Brown-Steiner, B., Jathar, S. H., Jimenez, J. L., Kreidenweis, S. M., Lonsdale, C.
575 R., Onasch, T. B., Ortega, A. M., and Pierce, J. R.: Aging Effects on Biomass Burning Aerosol Mass and Composition: A
576 Critical Review of Field and Laboratory Studies, *Environmental science & technology*, 53, 10007-10022,
577 10.1021/acs.est.9b02588, 2019.
- 578 Jiang, H., Frie, A. L., Lavi, A., Chen, J. Y., Zhang, H., Bahreini, R., and Lin, Y.-H.: Brown Carbon Formation from Nighttime
579 Chemistry of Unsaturated Heterocyclic Volatile Organic Compounds, *Environmental Science & Technology Letters*, 6, 184-
580 190, 10.1021/acs.estlett.9b00017, 2019.
- 581 Jo, D. S., Park, R. J., Lee, S., Kim, S. W., and Zhang, X.: A global simulation of brown carbon: implications for photochemistry
582 and direct radiative effect, *Atmos. Chem. Phys.*, 16, 3413-3432, 10.5194/acp-16-3413-2016, 2016.
- 583 Kasthuriarachchi, N. Y., Rivellini, L.-H., Adam, M. G., and Lee, A. K. Y.: Light Absorbing Properties of Primary and Secondary
584 Brown Carbon in a Tropical Urban Environment, *Environmental science & technology*, 54, 10808-10819,
585 10.1021/acs.est.0c02414, 2020.
- 586 Kodros, J. K., Papanastasiou, D. K., Paglione, M., Masiol, M., Squizzato, S., Florou, K., Skyllakou, K., Kaltsonoudis, C., Nenes,
587 A., and Pandis, S. N.: Rapid dark aging of biomass burning as an overlooked source of oxidized organic aerosol, *Proceedings*
588 *of the National Academy of Sciences*, 117, 33028-33033, doi:10.1073/pnas.2010365117, 2020.
- 589 Kodros, J. K., Kaltsonoudis, C., Paglione, M., Florou, K., Jorga, S., Vasilakopoulou, C., Cirtog, M., Cazaunau, M., Picquet-
590 Varrault, B., Nenes, A., and Pandis, S. N.: Secondary aerosol formation during the dark oxidation of residential biomass
591 burning emissions, *Environmental Science: Atmospheres*, 2, 1221-1236, 10.1039/D2EA00031H, 2022.
- 592 Kuang, Y., Xu, W., Tao, J., Ma, N., Zhao, C., and Shao, M.: A Review on Laboratory Studies and Field Measurements of
593 Atmospheric Organic Aerosol Hygroscopicity and Its Parameterization Based on Oxidation Levels, *Current Pollution*
594 *Reports*, 10.1007/s40726-020-00164-2, 2020.
- 595 Kuang, Y., Huang, S., Xue, B., Luo, B., Song, Q., Chen, W., Hu, W., Li, W., Zhao, P., Cai, M., Peng, Y., Qi, J., Li, T., Wang, S.,
596 Chen, D., Yue, D., Yuan, B., and Shao, M.: Contrasting effects of secondary organic aerosol formations on organic aerosol
597 hygroscopicity, *Atmos. Chem. Phys.*, 21, 10375-10391, 10.5194/acp-21-10375-2021, 2021.
- 598 Kumar, N. K., Corbin, J. C., Bruns, E. A., Massabó, D., Slowik, J. G., Drinovec, L., Močnik, G., Prati, P., Vlachou, A.,
599 Baltensperger, U., Gysel, M., El-Haddad, I., and Prévôt, A. S. H.: Production of particulate brown carbon during



- 600 atmospheric aging of residential wood-burning emissions, *Atmos. Chem. Phys.*, 18, 17843-17861, 10.5194/acp-18-17843-
601 2018, 2018.
- 602 Lareau, N. P., and Clements, C. B.: Environmental controls on pyrocumulus and pyrocumulonimbus initiation and
603 development, *Atmos. Chem. Phys.*, 16, 4005-4022, 10.5194/acp-16-4005-2016, 2016.
- 604 Laskin, A., Laskin, J., and Nizkorodov, S. A.: Chemistry of Atmospheric Brown Carbon, *Chemical Reviews*, 115, 4335-4382,
605 10.1021/cr5006167, 2015.
- 606 Li, C., He, Q., Hettiyadura, A. P. S., Käfer, U., Shmul, G., Meidan, D., Zimmermann, R., Brown, S. S., George, C., Laskin, A.,
607 and Rudich, Y.: Formation of Secondary Brown Carbon in Biomass Burning Aerosol Proxies through NO₃ Radical Reactions,
608 *Environmental science & technology*, 54, 1395-1405, 10.1021/acs.est.9b05641, 2020a.
- 609 Li, M., Wang, X., Lu, C., Li, R., Zhang, J., Dong, S., Yang, L., Xue, L., Chen, J., and Wang, W.: Nitrated phenols and the phenolic
610 precursors in the atmosphere in urban Jinan, China, *Science of The Total Environment*, 714, 136760,
611 <https://doi.org/10.1016/j.scitotenv.2020.136760>, 2020b.
- 612 Li, Z., Tan, H., Zheng, J., Liu, L., Qin, Y., Wang, N., Li, F., Li, Y., Cai, M., Ma, Y., and Chan, C. K.: Light absorption properties
613 and potential sources of particulate brown carbon in the Pearl River Delta region of China, *Atmos. Chem. Phys.*, 19, 11669-
614 11685, 10.5194/acp-19-11669-2019, 2019a.
- 615 Li, Z. J., Tan, H. B., Zheng, J., Liu, L., Qin, Y. M., Wang, N., Li, F., Li, Y. J., Cai, M. F., Ma, Y., and Chan, C. K.: Light absorption
616 properties and potential sources of particulate brown carbon in the Pearl River Delta region of China, *Atmospheric
617 Chemistry and Physics*, 19, 11669-11685, 10.5194/acp-19-11669-2019, 2019b.
- 618 Lin, P., Bluvshstein, N., Rudich, Y., Nizkorodov, S. A., Laskin, J., and Laskin, A.: Molecular Chemistry of Atmospheric Brown
619 Carbon Inferred from a Nationwide Biomass Burning Event, *Environmental science & technology*, 51, 11561-11570,
620 10.1021/acs.est.7b02276, 2017.
- 621 Liu, P., Kaplan, J. O., Mickley, L. J., Li, Y., Chellman, N. J., Arienzo, M. M., Kodros, J. K., Pierce, J. R., Sigl, M., Freitag, J.,
622 Mulvaney, R., Curran, M. A. J., and McConnell, J. R.: Improved estimates of preindustrial biomass burning reduce the
623 magnitude of aerosol climate forcing in the Southern Hemisphere, *Science Advances*, 7, 10.1126/sciadv.abc1379, 2021.
- 624 Liu, S., Ahlm, L., Day, D. A., Russell, L. M., Zhao, Y., Gentner, D. R., Weber, R. J., Goldstein, A. H., Jaoui, M., Offenberg, J. H.,
625 Kleindienst, T. E., Rubitschun, C., Surratt, J. D., Sheesley, R. J., and Scheller, S.: Secondary organic aerosol formation from
626 fossil fuel sources contribute majority of summertime organic mass at Bakersfield, *J. Geophys. Res. - Atmos.*, 117,
627 <https://doi.org/10.1029/2012JD018170>, 2012.
- 628 Liu, Y., Wang, T., Fang, X., Deng, Y., Cheng, H., Bacha, A. U., Nabi, I., and Zhang, L.: Brown carbon: An underlying driving
629 force for rapid atmospheric sulfate formation and haze event, *The Science of the total environment*, 734, 139415,
630 10.1016/j.scitotenv.2020.139415, 2020.
- 631 Luo, B., Kuang, Y., Huang, S., Song, Q., Hu, W., Li, W., Peng, Y., Chen, D., Yue, D., Yuan, B., and Shao, M.: Parameterizations
632 of size distribution and refractive index of biomass burning organic aerosol with black carbon content, *Atmos. Chem. Phys.*,
633 22, 12401-12415, 10.5194/acp-22-12401-2022, 2022.
- 634 Marufu, L., Dentener, F., Lelieveld, J., Andreae, M. O., and Helas, G.: Photochemistry of the African troposphere: Influence
635 of biomass-burning emissions, *Journal of Geophysical Research: Atmospheres*, 105, 14513-14530,
636 <https://doi.org/10.1029/1999JD901055>, 2000.
- 637 Mayorga, R. J., Zhao, Z., and Zhang, H.: Formation of secondary organic aerosol from nitrate radical oxidation of phenolic



- 638 VOCs: Implications for nitration mechanisms and brown carbon formation, *Atmospheric Environment*, 244, 117910,
639 <https://doi.org/10.1016/j.atmosenv.2020.117910>, 2021.
- 640 Palm, B. B., Peng, Q., Fredrickson, C. D., Lee, B. H., Garofalo, L. A., Pothier, M. A., Kreidenweis, S. M., Farmer, D. K., Pokhrel,
641 R. P., Shen, Y., Murphy, S. M., Permar, W., Hu, L., Campos, T. L., Hall, S. R., Ullmann, K., Zhang, X., Flocke, F., Fischer, E. V.,
642 and Thornton, J. A.: Quantification of organic aerosol and brown carbon evolution in fresh wildfire plumes, *Proceedings*
643 *of the National Academy of Sciences*, 202012218, 10.1073/pnas.2012218117, 2020.
- 644 Petters, M. D., Carrico, C. M., Kreidenweis, S. M., Prenni, A. J., DeMott, P. J., Collett Jr., J. L., and Moosmüller, H.: Cloud
645 condensation nucleation activity of biomass burning aerosol, *Journal of Geophysical Research: Atmospheres*, 114,
646 <https://doi.org/10.1029/2009JD012353>, 2009.
- 647 Price, C. L., Preston, T. C., and Davies, J. F.: Hygroscopic Growth, Phase Morphology, and Optical Properties of Model
648 Aqueous Brown Carbon Aerosol, *Environmental science & technology*, 56, 3941-3951, 10.1021/acs.est.1c07356, 2022.
- 649 Qin, Y. M., Tan, H. B., Li, Y. J., Li, Z. J., Schurman, M. I., Liu, L., Wu, C., and Chan, C. K.: Chemical characteristics of brown
650 carbon in atmospheric particles at a suburban site near Guangzhou, China, *Atmos. Chem. Phys.*, 18, 16409-16418,
651 10.5194/acp-18-16409-2018, 2018.
- 652 Rana, M. S., and Guzman, M. I.: Oxidation of Catechols at the Air–Water Interface by Nitrate Radicals, *Environmental*
653 *science & technology*, 56, 15437-15448, 10.1021/acs.est.2c05640, 2022.
- 654 Running, S. W.: Is Global Warming Causing More, Larger Wildfires?, *Science*, 313, 927, 10.1126/science.1130370, 2006.
- 655 Saleh, R., Hennigan, C. J., McMeeking, G. R., Chuang, W. K., Robinson, E. S., Coe, H., Donahue, N. M., and Robinson, A. L.:
656 Absorptivity of brown carbon in fresh and photo-chemically aged biomass-burning emissions, *Atmos. Chem. Phys.*, 13,
657 7683-7693, 10.5194/acp-13-7683-2013, 2013.
- 658 Saleh, R.: From Measurements to Models: Toward Accurate Representation of Brown Carbon in Climate Calculations,
659 *Current Pollution Reports*, 6, 90-104, 10.1007/s40726-020-00139-3, 2020.
- 660 Selimovic, V., Yokelson, R. J., McMeeking, G. R., and Coefield, S.: Aerosol Mass and Optical Properties, Smoke Influence
661 on O₃, and High NO₃ Production Rates in a Western U.S. City Impacted by Wildfires, *Journal of Geophysical Research:*
662 *Atmospheres*, 125, e2020JD032791, <https://doi.org/10.1029/2020JD032791>, 2020.
- 663 Song, M., Liu, X., Zhang, Y., Shao, M., Lu, K., Tan, Q., Feng, M., and Qu, Y.: Sources and abatement mechanisms of VOCs in
664 southern China, *Atmospheric Environment*, 201, 28-40, <https://doi.org/10.1016/j.atmosenv.2018.12.019>, 2019.
- 665 Stockwell, C. E., Veres, P. R., Williams, J., and Yokelson, R. J.: Characterization of biomass burning emissions from cooking
666 fires, peat, crop residue, and other fuels with high-resolution proton-transfer-reaction time-of-flight mass spectrometry,
667 *Atmos. Chem. Phys.*, 15, 845-865, 10.5194/acp-15-845-2015, 2015.
- 668 Tiitta, P., Leskinen, A., Hao, L., Yli-Pirilä, P., Kortelainen, M., Grigonyte, J., Tissari, J., Lamberg, H., Hartikainen, A., Kuuspallo,
669 K., Kortelainen, A. M., Virtanen, A., Lehtinen, K. E. J., Komppula, M., Pieber, S., Prévôt, A. S. H., Onasch, T. B., Worsnop, D.
670 R., Czech, H., Zimmermann, R., Jokiniemi, J., and Sippula, O.: Transformation of logwood combustion emissions in a smog
671 chamber: formation of secondary organic aerosol and changes in the primary organic aerosol upon daytime and nighttime
672 aging, *Atmos. Chem. Phys.*, 16, 13251-13269, 10.5194/acp-16-13251-2016, 2016.
- 673 Tong, Y., Pospisilova, V., Qi, L., Duan, J., Gu, Y., Kumar, V., Rai, P., Stefanelli, G., Wang, L., Wang, Y., Zhong, H., Baltensperger,
674 U., Cao, J., Huang, R. J., Prévôt, A. S. H., and Slowik, J. G.: Quantification of solid fuel combustion and aqueous chemistry
675 contributions to secondary organic aerosol during wintertime haze events in Beijing, *Atmos. Chem. Phys.*, 21, 9859-9886,



- 676 10.5194/acp-21-9859-2021, 2021.
- 677 van der Werf, G. R., Randerson, J. T., Giglio, L., van Leeuwen, T. T., Chen, Y., Rogers, B. M., Mu, M., van Marle, M. J. E.,
678 Morton, D. C., Collatz, G. J., Yokelson, R. J., and Kasibhatla, P. S.: Global fire emissions estimates during 1997–2016, *Earth*
679 *Syst. Sci. Data*, 9, 697–720, 10.5194/essd-9-697-2017, 2017.
- 680 Wang, J., Nie, W., Cheng, Y., Shen, Y., Chi, X., Wang, J., Huang, X., Xie, Y., Sun, P., Xu, Z., Qi, X., Su, H., and Ding, A.: Light
681 absorption of brown carbon in eastern China based on 3-year multi-wavelength aerosol optical property observations and
682 an improved absorption Ångström exponent segregation method, *Atmos. Chem. Phys.*, 18, 9061–9074, 10.5194/acp-18-
683 9061-2018, 2018a.
- 684 Wang, J., Shilling, J. E., Liu, J., Zelenyuk, A., Bell, D. M., Petters, M. D., Thalman, R., Mei, F., Zaveri, R. A., and Zheng, G.:
685 Cloud droplet activation of secondary organic aerosol is mainly controlled by molecular weight, not water solubility, *Atmos.*
686 *Chem. Phys.*, 19, 941–954, 10.5194/acp-19-941-2019, 2019a.
- 687 Wang, J., Ye, J., Zhang, Q., Zhao, J., Wu, Y., Li, J., Liu, D., Li, W., Zhang, Y., Wu, C., Xie, C., Qin, Y., Lei, Y., Huang, X., Guo, J.,
688 Liu, P., Fu, P., Li, Y., Lee, H. C., Choi, H., Zhang, J., Liao, H., Chen, M., Sun, Y., Ge, X., Martin, S. T., and Jacob, D. J.: Aqueous
689 production of secondary organic aerosol from fossil-fuel emissions in winter Beijing haze, *Proceedings of the National*
690 *Academy of Sciences*, 118, e2022179118, 10.1073/pnas.2022179118, 2021.
- 691 Wang, Q., Saturno, J., Chi, X., Walter, D., Lavric, J. V., Moran-Zuloaga, D., Ditas, F., Pöhlker, C., Brito, J., Carbone, S., Artaxo,
692 P., and Andreae, M. O.: Modeling investigation of light-absorbing aerosols in the Amazon Basin during the wet season,
693 *Atmos. Chem. Phys.*, 16, 14775–14794, 10.5194/acp-16-14775-2016, 2016.
- 694 Wang, Q., Ye, J., Wang, Y., Zhang, T., Ran, W., Wu, Y., Tian, J., Li, L., Zhou, Y., Hang Ho, S. S., Dang, B., Zhang, Q., Zhang, R.,
695 Chen, Y., Zhu, C., and Cao, J.: Wintertime Optical Properties of Primary and Secondary Brown Carbon at a Regional Site in
696 the North China Plain, *Environmental science & technology*, 53, 12389–12397, 10.1021/acs.est.9b03406, 2019b.
- 697 Wang, S.-C., Wang, Y., Estes, M., Lei, R., Talbot, R., Zhu, L., and Hou, P.: Transport of Central American Fire Emissions to the
698 U.S. Gulf Coast: Climatological Pathways and Impacts on Ozone and PM_{2.5}, *Journal of Geophysical Research: Atmospheres*,
699 123, 8344–8361, <https://doi.org/10.1029/2018JD028684>, 2018b.
- 700 Wang, Y., Hu, M., Wang, Y., Zheng, J., Shang, D., Yang, Y., Liu, Y., Li, X., Tang, R., Zhu, W., Du, Z., Wu, Y., Guo, S., Wu, Z., Lou,
701 S., Hallquist, M., and Yu, J. Z.: The formation of nitro-aromatic compounds under high
702 NO_x and anthropogenic VOC conditions in urban Beijing, China, *Atmospheric*
703 *Chemistry and Physics*, 19, 7649–7665, 10.5194/acp-19-7649-2019, 2019c.
- 704 Wang, Y., Qiu, T., Zhang, C., Hao, T., Mabato, B. R. G., Zhang, R., Gen, M., Chan, M. N., Huang, D. D., Ge, X., Wang, J., Du,
705 L., Huang, R.-J., Chen, Q., Hoi, K. I., Mok, K. M., Chan, C. K., and Li, Y. J.: Co-photolysis of mixed chromophores affects
706 atmospheric lifetimes of brown carbon, *Environmental Science: Atmospheres*, 3, 1145–1158, 10.1039/D3EA00073G, 2023.
- 707 Wu, L., Huang, S., Liu, Y., Song, Q., Hu, W., Chen, W., Kuang, Y., Wang, X., Li, W., Peng, Y., Chen, D., Yue, D., Song, W., Yuan,
708 B., Wang, X., and Shao, M.: Source, formation mechanism and inhalation deposition flux of organic aerosols in urban and
709 rural areas of the Pearl River Delta, *Acta Scientiae Circumstantiae*, 44, 15–28, 10.13671/j.hjkxxb.2023.0194, 2024.
- 710 Yang, S., Yuan, B., Peng, Y., Huang, S., Chen, W., Hu, W., Pei, C., Zhou, J., Parrish, D. D., Wang, W., He, X., Cheng, C., Li, X.
711 B., Yang, X., Song, Y., Wang, H., Qi, J., Wang, B., Wang, C., Wang, C., Wang, Z., Li, T., Zheng, E., Wang, S., Wu, C., Cai, M.,
712 Ye, C., Song, W., Cheng, P., Chen, D., Wang, X., Zhang, Z., Wang, X., Zheng, J., and Shao, M.: The formation and mitigation
713 of nitrate pollution: comparison between urban and suburban environments, *Atmos. Chem. Phys.*, 22, 4539–4556,
714 10.5194/acp-22-4539-2022, 2022.



715 Yu, P., Toon, O. B., Bardeen, C. G., Zhu, Y., Rosenlof, K. H., Portmann, R. W., Thornberry, T. D., Gao, R.-S., Davis, S. M., Wolf,
716 E. T., de Gouw, J., Peterson, D. A., Fromm, M. D., and Robock, A.: Black carbon lofts wildfire smoke high into the
717 stratosphere to form a persistent plume, *Science*, 365, 587, [10.1126/science.aax1748](https://doi.org/10.1126/science.aax1748), 2019.

718 Yu, P., Davis, S. M., Toon, O. B., Portmann, R. W., Bardeen, C. G., Barnes, J. E., Telg, H., Maloney, C., and Rosenlof, K. H.:
719 Persistent Stratospheric Warming Due to 2019–2020 Australian Wildfire Smoke, *Geophysical Research Letters*, 48,
720 e2021GL092609, <https://doi.org/10.1029/2021GL092609>, 2021.

721 Ziemke, J. R., Chandra, S., Duncan, B. N., Schoeberl, M. R., Torres, O., Damon, M. R., and Bhartia, P. K.: Recent biomass
722 burning in the tropics and related changes in tropospheric ozone, *Geophysical Research Letters*, 36,
723 <https://doi.org/10.1029/2009GL039303>, 2009.

724